AIAA 2013-1866

Remote Charging Mechanics for Electrostatic Inflation of Membrane Space Structures

Laura A. Stiles, Zoltan Sternovsky and Hanspeter Schaub

University of Colorado, Boulder, CO 80309-0431

AIAA Gossamer Systems Forum
April 8-11, 2013 / Boston, MA

Remote Charging Mechanics for Electrostatic Inflation of Membrane Space Structures

Laura A. Stiles,* Zoltan Sternovsky† and Hanspeter Schaub‡
University of Colorado, Boulder, CO 80309-0431

The mechanics of remotely charging a membrane space structure in a vacuum environment are explored. This research supports the investigation of Electrostatically Inflated Membrane space Structures (EIMS). EIMS uses repulsive electrostatic pressure to tension layers of membrane materials to form a self-supporting space structure. How to remotely charge the membrane structure via an electron beam is studied through analysis and supplemented by experiment results. The experiments performed seek to characterize the yield curve for secondary electron emission for several membrane materials (such as aluminized Mylar). The experimental setup is presented and initial test results are discussed.

I. Introduction

Gossamer structures are lightweight, compactable structures that offer significant mass and volume savings from traditional spacecraft systems. These lightweight structures are envisioned for a variety of space applications such as communications reflectors, drag devices, or solar sails. Within the class of gossamer structures are inflatable space structures, which can utilize methods such as pressurized gas, sublimating chemicals, or evaporating liquids for inflation.[?] Alternatively, the concept of electrostatic pressure for inflation is explored in Reference **?**. Electrostatic inflation uses repulsive electrostatic forces between layers of membrane materials to inflate to a stable, self-supporting space structure. Membrane layers are connected to limit inflation distance and shape the structures. The concept of an Electrostatically Inflated of Membrane space Structure (EIMS) is illustrated in Figure 1. EIMS share the benefits of low-mass and compact stowage with the classical inflatable structure, but does not suffer from sensitivity to puncture or the requirement for a closed shape. The electrostatic inflation concept is particularly applicable to structures such as arrays, solar power reflectors, or drag augmentation devices for de-orbiting and space debris avoidance purposes.

The novel concept of electrostatic inflation of membrane space structures is explored in References ?, **?**, and **?**. Previous EIMS research explores topics of voltage requirements to offset orbital perturbations, charge flux interactions, and EIMS as a radiation shielding device. The analysis in these previous papers concerns the voltage required on a two-membrane layered structure to offset normal compressive orbital perturbations to the inflated structure to maintain the inflated shape. In GEO, solar radiation pressure is the dominant compression pressure of the orbital perturbations. In LEO, solar radiation pressure dominates until an orbit altitude of approximately 500km, under which atmospheric drag becomes the dominant pressure. The potentials on the membranes must be high enough to produce sufficient electrostatic pressures to offset these compressive differential forces which would be experienced in orbit in order to keep the structure inflated. As no analytical solution to this electrostatic problem exists, numerical solutions were required to understand charge densities and corresponding potentials on the membranes. To offset the normal compressive orbital pressures, it was found that hundreds of Volts are required in GEO and a few kiloVolts in LEO.

Many challenges to the electrostatic inflation concept exist, such as plasma Debye shielding, space weather, orbital perturbations which may tend to collapse the structure, and complex structural dynamics. In Reference **?**, plasma

*Graduate Research Assistant, Aerospace Engineering Sciences Department, University of Colorado, Boulder, CO. AIAA student member, AAS student member

†Assistant Professor, Aerospace Engineering Sciences Department, University of Colorado, Boulder, CO.

‡Associate Professor, H. Joseph Smead Fellow, Aerospace Engineering Sciences Department, University of Colorado, Boulder, CO. AIAA Associate Fellow, AAS member

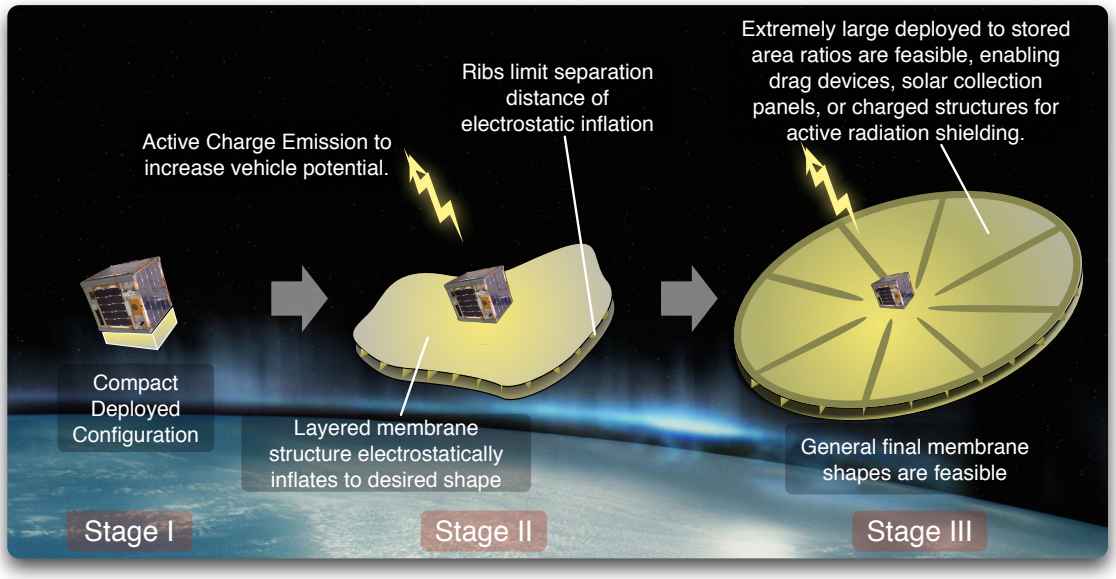

Figure 1: Electrostatic inflation concept illustration.

effects on EIMS are discussed in relation to the Debye shielding phenomenon. In the space plasma environment, electrons and ions rearrange to maintain macroscopic neutrality when perturbed by an external electric field.[?] This phenomena causes a steeper dropoff in the electrostatic potential surrounding a charged object than would occur in a vacuum. The Debye length is a measure of the shielding due to the plasma, signifying the distance at which a charged object is essentially shielded. In the Geostationary orbit (GEO) regime, the Debye length is nominally on the order of hundreds of meters, dependent on the changing electron and ion temperature and number density.[?] In low Earth orbit (LEO), however, the plasma is much more dense and the Debye length is generally on the order of millimeters or centimeters.[?] The LEO environment can therefore be a challenging environment for EIMS due to the limited distances for electrostatic actuation. Numerical simulations, however, show that the actual 'effective' Debye length can be more than an order of magnitude larger than the classically predicted Debye length in LEO when spacecraft are charged to high potentials.[?]

In addition to the analytical and numerical exploration of the EIMS concept, laboratory demonstrations have been built to demonstrate electrostatic inflation. These show that a few kilovolts can inflate a membrane structure over the compressive force of 1-g of gravity. This is illustrated in Figure 2 where a membrane structure is deployed from a compact configuration to a stable structure with only electrostatic pressure from charging to a few kiloVolts. As inflation in atmospheric conditions suffers from interactions with the air, demonstrations were moved to a vacuum environment in which inflation was demonstrated with lower potential levels than in atmospheric conditions. Also within the vacuum environment, the response to charge bombardment was explored, including studying dynamic response to the charge bombardment and the charge shielding capability of the structure.

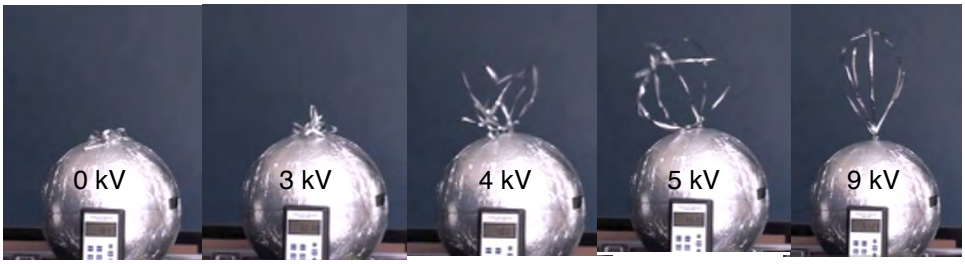

Figure 2: Electrostatic inflation of a gossamer structure

To achieve desired charge levels for electrostatic inflation, active charge emission, a high voltage power supply,

or remote charging are being considered. In this paper, the remote-charging scenario for EIMS is considered. Here, an electron beam is used to bombard the surface with electrons and change the absolute potential. The resulting potential from the beam depends on the energy of the electron beam, the secondary electron emission, the backscattered electrons, and the material being bombarded, as well as other charging phenomena, such as the ambient plasma ions and electrons and photoemission. This paper describes research concerning the secondary electron emission for EIMS-applicable materials such as aluminized Mylar and aluminized Kapton. Previous research has explored secondary electron emission for many materials. Experiments have been designed to measure secondary electron emission and theories have been empirically determined to model secondary yields. There haven't, however, been experiments to quantify secondary yields from metal-coated membrane materials, such as Aluminized Mylar. In this research, an experiment is designed and executed to experimentally determine the secondary yields for several EIMS-applicable materials. Fully understanding the secondary yield characteristics is critical to a full understanding of charging behavior and designing an EIMS system.

The research performed is also applicable to other spacecraft mission scenarios, for example the electrostatic re-orbiter concept. In this concept, an electrostatically charged space tug uses Coulomb forces to manipulate the orbit of a space debris object.[?] The space debris object will be naturally charged from the space environment, but the charge level can be augmented by remote charge transfer via a stream of charged particles. This research on remote charging may contribute to understanding how charging is more effectively performed for electrostatic re-orbiting based on the secondary electron contribution to charging.

In this paper, the background on spacecraft charging and secondary electron emission is first presented. Next, the designed experimental hardware and procedures to measure secondary electron emission are described. Experiments first performed use a well characterized material (Nickel) in order to better understand measurements and quantify any discrepancies from theory (for example due to ionization or measuring other secondary electrons). Finally, preliminary results are presented for membrane materials of Aluminized Mylar and Aluminized Kapton. The paper concludes by discussing the application of the experiment to the EIMS system.

II. Background

The ambient space plasma surrounding a spacecraft will cause the craft to obtain a non-zero potential with reference to the plasma. Based on the plasma and sunlight conditions, the craft can naturally become either positive or negative, with natural charging levels recorded up to -19 kV on the ATS-6 spacecraft.[?] The naturally occurring currents to the craft which cause charging include the plasma ion and electron flux, photoemission, secondary electron emission, and backscattered electrons.[?] The current balance equation is expressed as a sum of the following currents:

$$I_e(\phi) - I_s(\phi) - I_b(\phi) - I_{ph}(\phi) - I_i(\phi) = 0 \tag{1}$$

where I_e and I_i are the electron current and ion current from the plasma environment, I_b represents backscattered electron current, I_{ph} represents the emitted photoelectrons, and I_s is the secondary electron emission current. Currents can also be actively induced by charged beam emission or charge beam impact. With beam emission, the outgoing charged particles become a part of the current balance given in Equation (1). Emitting ions can charge the spacecraft negatively while electron emission can induce positive charging. For charging by beam impact, the resulting charge levels depend on the energy of the incoming electrons, secondary and backscatter electron levels, and how the surface is initially charged.[?]

It is important to understand the secondary electron yield to determine how the spacecraft will be charged using electron beam impact. Secondary emission occurs when an incoming electron shares energy with nearby electrons in a material and the energy is enough for the electron to leave the surface. The energy of the secondary electrons is usually only a few eV.[?] The secondary electron yield coefficient, δ, is defined as the ratio of outgoing electrons (from secondary emission) to the current of incoming electrons. The outgoing electrons are referred to as I_{SEE}, describing the secondary electrons emitted from a material sample being bombarded by incoming electrons. I_{beam} is the incoming current from the electron source. The secondary electron yield is therefore defined as:

$$\delta = \frac{I_{\text{SEE}}}{I_{\text{beam}}} \tag{2}$$

A theoretical model for the secondary yield, δ is described by Sternglass[?] by Equation 3. The equation is based on

fits to empirical data for many materials.

$$\delta(E_0) = 7.4\delta_{max}\frac{E_0}{E_{0,max}}e^{-2\sqrt{\frac{E_0}{E_{0,max}}}} \tag{3}$$

Here, E_0 is the energy of the incoming electron beam. The maximum value for secondary yield is described with δ_{max} and the energy at which this maximum occurs is $E_{0,max}$. These maxima depend on the material being bombarded by electrons. The secondary yield is therefore a function of only beam energy and material. The Sternglass curve is illustrated generally in Figure 3. What is interesting to note here is that there are two unity crossings. Between

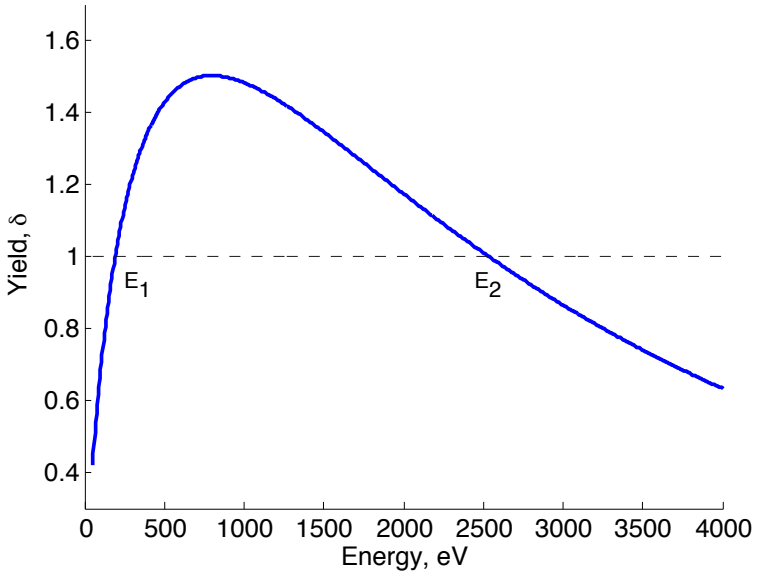

Figure 3: Illustration of secondary electron emission yield curve

energies E_1 and E_2, the number of electrons leaving the material due to secondary emission is higher than the number of incoming electrons. Although intuitively a surface would charge negatively through electron impact, if the beam energy lies between energies E_1 and E_2, the surface would charge positively due to the greater number of electron leaving than arriving.

To illustrate the effect of materials on secondary electron emission and spacecraft charging, Figure 4 is shown. In this figure, various currents are represented. First, the environmental currents are plotted for a nominal geosynchronous orbit (GEO). It is assumed that the spacecraft is in sunlight, thus the currents included here are the photoelectron current, plasma electron current, and the ram ion current. Next the current from a remote charging electron beam is included, assuming an energy of 20 keV. Included next are the secondary electron emission from two different materials: Aluminum and Kapton. The two materials have different yield properties, thus the resulting currents can vary drastically. Lastly, the sum of all currents to the spacecraft are illustrated for the two different materials cases. As can be seen in the Figure, the equilibrium where the currents sum to zero occur several thousand volts apart. Th difference demonstrates how important it is to correctly quantify the secondary electron emission to understand how a spacecraft will charge when using remote charging.

The parameters of δ_{max} and $E_{0,max}$ to determine the secondary electron yield can be determined through experiment or simulation.[?] Some examples of the yield parameters for various materials are shown in Table 1. It can be seen that there is a significant difference in the yield parameters of metals and polymers. In general, insulators have higher secondary electron yields than conductive materials.[?]

In this research, an experimental procedure is used to better understand the secondary emission yield for materials applicable to EIMS, some of which have not been previously determined via experiment. What is of interest is whether the metal-coated polymers, such as aluminized Mylar or aluminized Kapton, have yield parameters more similar to metals or to polymers.

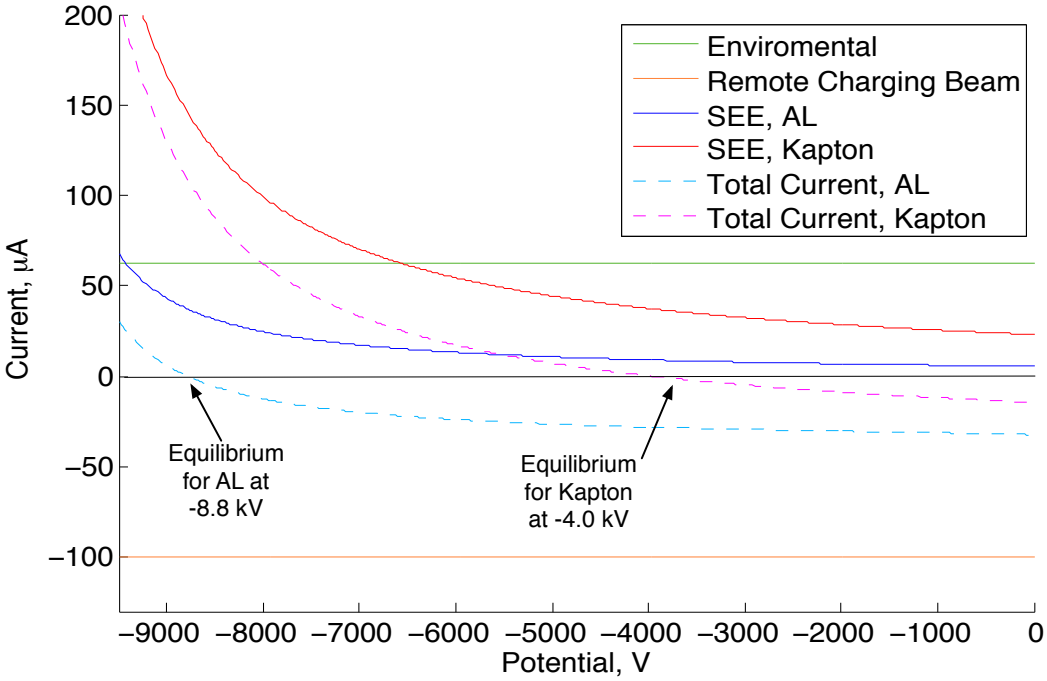

Figure 4: Illustration of effect of secondary electron emission on spacecraft charging

Table 1: Secondary emission yield parameters for selected materials

	$E_{0,max}(eV)$	δ_{max}
Aluminum[?]	300	0.95
Nickel[?]	500	1.3
Copper[?]	600	1.3
Kapton[?]	150	2.1
Mylar[?]	175	4.8

III. Experiment Description

The purpose of the experiment is to investigate the secondary electron emission from samples of aluminized Mylar and aluminized Kapton to better understand the remote charging response of these EIMS-applicable materials. Initially, a baseline experiment with a Nickel material sample is performed to compare the experimental results of secondary emission to the accepted values for Nickel. Then, EIMS-applicable materials are studied to determine secondary yield characteristics. The yields of these materials have not previously been experimentally determined.

A. Hardware Description

The hardware setup for the remote charging experiments includes an electron gun emitting charge toward a material sample inside a vacuum chamber. The vacuum chamber within which the experiments take place is shown in Figure 5. The chamber has vacuum capability down to approximately 10^{-7} Torr. Each of the hardware components of the setup are described below.

An electron gun is used to emit electrons which are accelerated toward the membrane sample. A filament is heated and electrons which are thermionically emitted are accelerated off by the electrostatic field between the filament and a grounded wire mesh.The electron gun filament is constructed of 5mil coiled Tungsten wire. The electron gun can operate with energies up to 5 keV and emit current up to 5 mA.

The mounting system for the material sample is illustrated in the diagram shown in Figure 6. The sample and grids are mounted inside a shielding 2 inch diameter copper pipe which is grounded via connection to the vacuum chamber

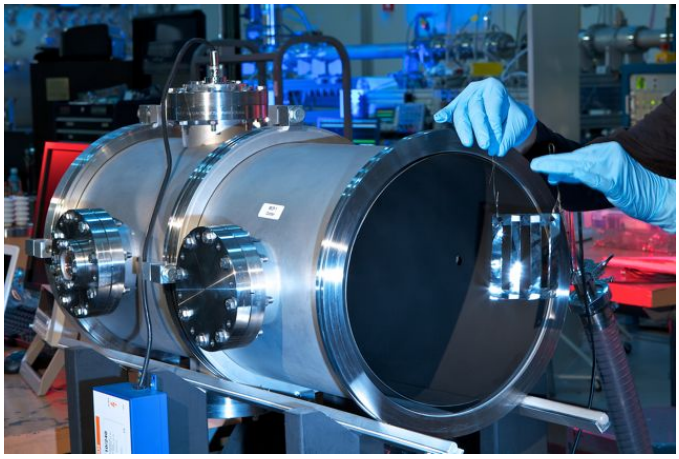

Figure 5: Vacuum chamber used for charging experiments

walls. The material sample is mounted on an 1.25 inch aluminum plate, shown in Figure 8(b). Ceramic mounts and other insulating materials (Teflon, Kapton) are used to keep the sample mount and grids electrically isolated from the grounded metal cup. Each grid and the sample mount have individual electrical connections through an electrical feedthrough in the chamber to allow individual biasing. The setup as viewed from outside the vacuum chamber is shown in Figure7.

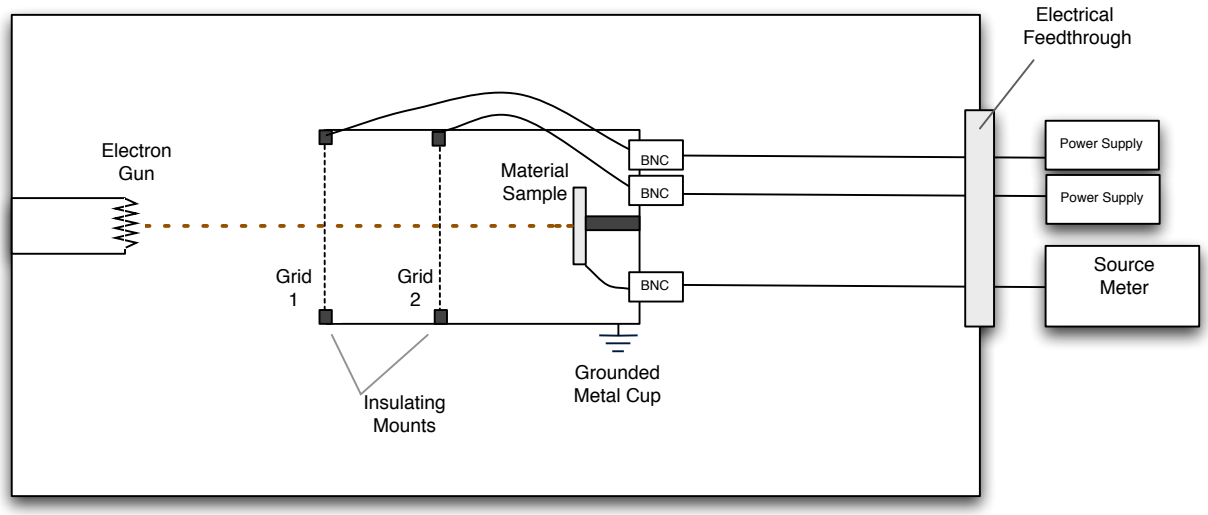

Figure 6: Experimental setup for measuring secondary electron emission

The material sample is connected to a Kiethley Model 6487 PicoAmmeter/Voltage Source (source-meter). This model has $\pm$500V DC voltage source and current measurement capabilities. The source-meter is used to simultaneously run through a pre-defined voltage sweep while measuring current. This sweep is used for the characterization of the I-V curve in order to determine the current from the material sample and the beam current, as will be further explained in the following section.

B. Experiment Procedure

To determine the secondary electron yield curve for a material (as shown in Figure 3), the following experimental procedures are performed at a range of primary electron energies. The yield curve is constructed point by point, calculating the yield at many primary electron energies.The range capability for electron energies to be explored is from 100 eV up to 5 keV with the hardware setup described above.

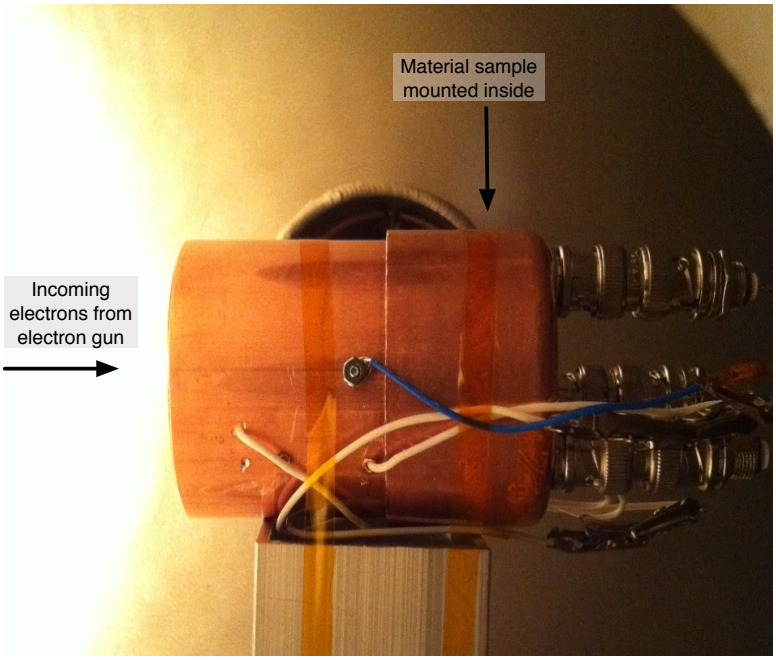

Figure 7: Experimental setup for measuring secondary electron emission

a) Aluminum grid inside test apparatus (view in primary electron velocity direction)

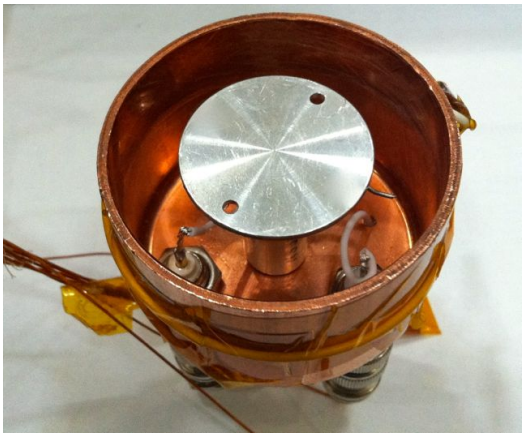

b) Aluminum mount for affixing material samples inside test apparatus (behind grid shown in A)

Figure 8: Sample mount apparatus

To calculate the yield, equation (2) is employed. It is necessary to experimentally determine both the beam current and the sample current for this equation. Each of these quantities can be found for the particular electron energy by sweeping a voltage on the material sample and simultaneously measuring the currents using the Kiethley source-meter. The voltage sweep is chosen to range from -50 V to 50 V to capture the full behavior of I-V curve. Figure 9 shows what the measurement from the voltage sweep looks like.

The current on the material sample being measured by the SourceMeter is a combination of several currents: primary electrons from the electron gun, secondary electrons emitted from the material sample, secondary electrons emitted from the grids, and ions from the ionization of the water and nitrogen molecules in the chamber. First, the main source of current is the primary electrons from the electron gun. The current emitted from the gun for the experiments is 3 mA. The electron gun provides a spray of electron from the spiral filament with minimal directionality, therefore only a fraction of the 3 mA reaches the material sample. The beam current which reaches the sample can be approximated

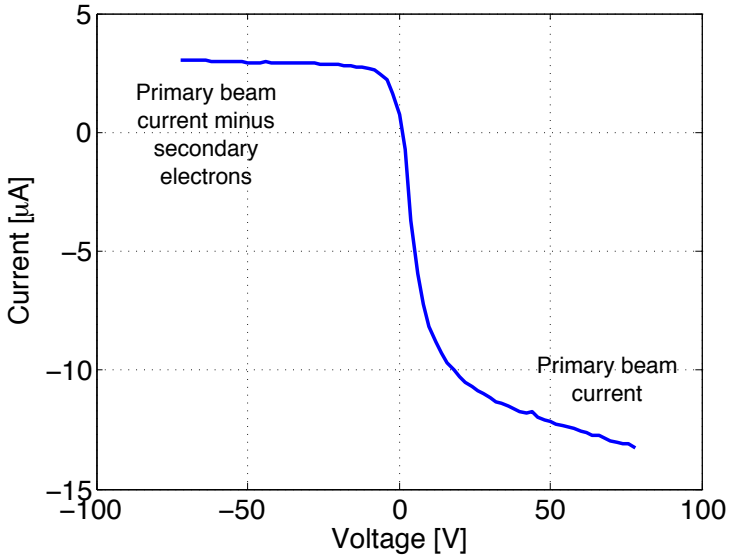

Figure 9: Current vs. voltage data sample

from the positive potential data of the I-V curve shown in Figure 9. When the sample is biased positively to a level greater than the energy of the secondary electrons (which are only a few eV), all secondary electrons are attracted back to the sample. The current of leaving secondaries is cancelled out by the incoming current of secondaries immediately returning. The primary beam is unaffected here, as the energy of the beam is a minimum of 100 eV. The positive end of the I-V curve therefore gives us the value of I_{beam} for Equation (2) and is expressed as:

$$I_{+\phi} = I_{beam} \tag{4}$$

At the opposite end of the I-V curve where the bias potential on the sample is negative, the currents being measured are the beam current minus the secondary electrons leaving the material sample. Because the sample is biased negatively, all the lower energy secondary electrons which are emitted from the material are accelerated away due to electrostatic repulsion. As the beam current is already determined as described above, the secondary electron current can be calculated from the measurement. Recall from Equation (2) that the current of the secondary electrons can be rewritten as:

$$I_{SEE} = \delta I_{beam} \tag{5}$$

Therefore the measured current at negative potentials, named $I_{-\phi}$, can be defined as:

$$I_{-\phi} = I_{beam} + I_{SEE} = I_{beam}(1 + \delta) \tag{6}$$

By calculating the ratio ($\mathcal{R}$) of the current at the two ends of the I-V curve:

$$\mathcal{R} = \frac{I_{-\phi}}{I_{+\phi}} = \frac{I_{beam}(1 + \delta)}{I_{beam}} = 1 - \delta \tag{7}$$

we can solve for the secondary yield:

$$\delta = 1 - \mathcal{R} \tag{8}$$

Thus, the secondary electron emission yield at a particular primary electron energy can be calculated directly from the measurement of the I-V curve. This calculation determines one point on the yield curve for the material under study. Repeating the procedure and this calculation at a range of primary electron energies, the yield curve for a material is constructed.

IV. Experimental Results

In this section, the preliminary experimental results for baseline materials and membrane materials are presented and discussed.

A. Baseline measurements

In order to verify the experimental setup and procedures, a sample of Nickel was chosen as the first material to study. Nickel has known secondary electron emission characteristics through experiment.[?] Nickel also makes a good material for this procedure due to the slow oxidation rate or corrosion resistance, as oxidation can have a significant effect on secondary emission.

In the current stage of the experiment, there remain deviations between the experimentally determined yield curve for Nickel and the accepted Sternglass curve. There are several reasons why the data may deviate from the theory. First, the material sample may be collecting secondary electrons being emitted from the grids or from other surfaces inside the apparatus. To test this theory, different biases were added to the inner and outer grids. The purpose of biasing the grids to a positive bias voltage is to recollect the secondary electrons that may be ejected from the grids. The biasing effects on the inner and outer grid are shown in Figure 10. The biasing of the grids has an effect on the yield values, though does not greatly affect the trend of the experimental data. It is therefore concluded that other effects are likely contributing to the deviation from theory.

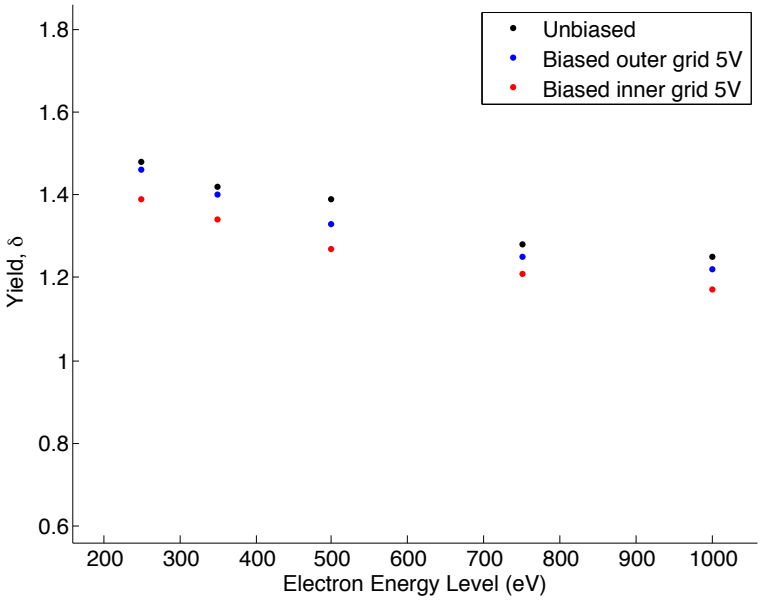

Figure 10: Experimental data using grid biasing

A second phenomenon which affects the measurement of secondary electrons is ionization. Here, a primary electron impacts a molecule (primarily water vapor or Nitrogen in the vacuum chamber) and ejects an electron, thus creating an ion. The ion may be collected by the sample if the material is biased to a negative potential, thus attracting the positively charged ions. To calculate the approximate number of ions being created by impact ionization, the following equation is employed:[?]

$$I_i = I_0 N q_i x \tag{9}$$

In Equation (9), I_0 represents the electron beam current, N represents the number density of the gas in the chamber, q_i is the ionization cross section, and x is the mean free path length. Cross sections of molecules can be found in the NIST online database for ionization cross section by electron impact (See Reference **?**). The cross section is dependent on the incoming electron energy and reaches a maximum near 150 eV. It is assumed that the primary molecule in the chamber is water, thus ionization cross sections for H_2O are used in calculations. Based on the parameters given in Table 2, the ion current is on the order of 0.1 to 0.6 μA. The currents measured for the yield calculations are on the

order of microAmps, therefore the ionization of molecules may have a noticeable effect on the measurements and thus the yield curve.

Table 2: Parameters for calculating ion currents from impact ionization (example at 150 eV)

Beam current, i_0	13 μA
Number density, N	2.3e+17 1/m^3
Mean free path length, x	7.3 m
Cross section, q_i	2.7e-20 m^2
Ion current, i_i	0.58 μA

Another known issue with the Nickel sample is a non-flat surface. The Sternglass yield curve assumes a flat plate and the sample used has a noticeable curvature obtained when cutting the material. The next steps in the effort to understand the data are to obtain a non-curved Nickel sample, study the affect of adjusting the grids, or adjust the electron beam to a more directed stream to help minimize secondary emission from other parts of the test apparatus.

B. Membrane Materials

While efforts continue to understand and quantify the discrepancy between the theory and experiment for the Nickel material, preliminary experiments are being conducted with membrane materials. The first material in this study is Aluminized Mylar. The sample is 1/4 mil thickness Aluminized Mylar. Figure 11 shows the yield curve that was built with experimental data. The data is compared to the Sternglass yield curves for both Aluminum and Kapton. As predicted, the Aluminized Mylar lies between the two pure materials. While this data is preliminary, the trend of the data follows the shape of Sternglass curve. Fitting a Sternglass curve to the data gives a maximum energy near 375 eV and a maximum secondary yield near 2.4.

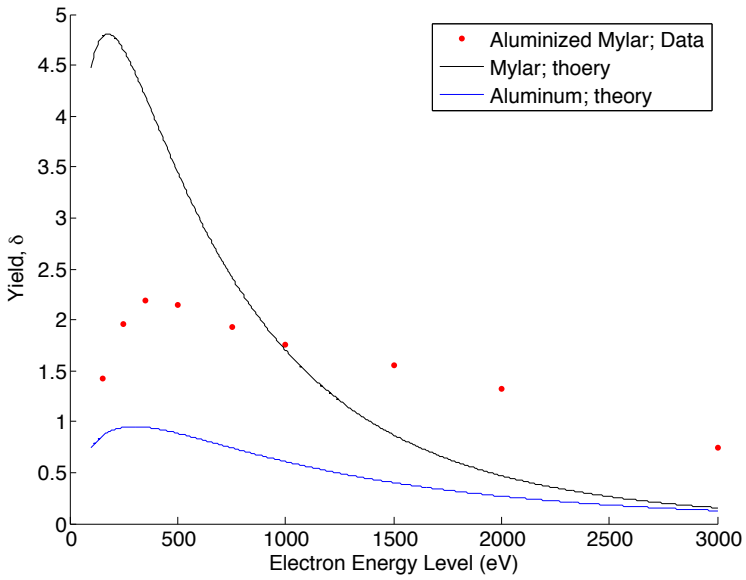

Figure 11: Experimental data for Aluminized Mylar compared the Sternglass model for Aluminum and Mylar

Aluminized Kapton is also studied and a preliminary yield curve presented in Figure 12. The data again follows the general shape of a Sternglass curve showing a peak at low energies and the yield decreasing as energies become larger. Here, the maximum energy is near 250 eV and the maximum yield near 2.1.

As this data is only preliminary, conclusions are not yet drawn about the magnitudes of the yield values or energy maxima. What can be studied, though, is the comparison between the two membrane material data sets, as presented in Figure 12. The Aluminized Kapton yield curve is similar to that of Aluminized Mylar, suggesting that there may be little difference in remote charging behavior with these two membrane materials. At nearly every energy, the Aluminized Mylar shows a slightly higher yield value. For both of the membrane materials, the yield is above unity

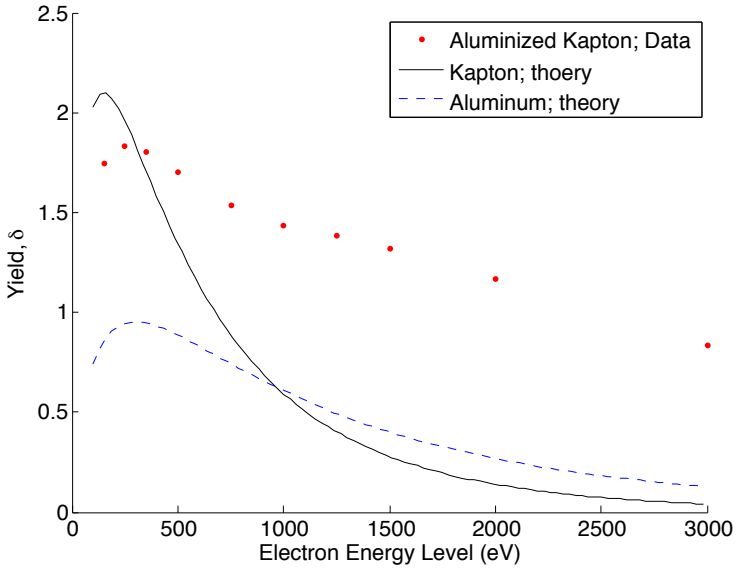

Figure 12: Experimental data for Aluminized Kapton compared the Sternglass model for Aluminum and Kapton

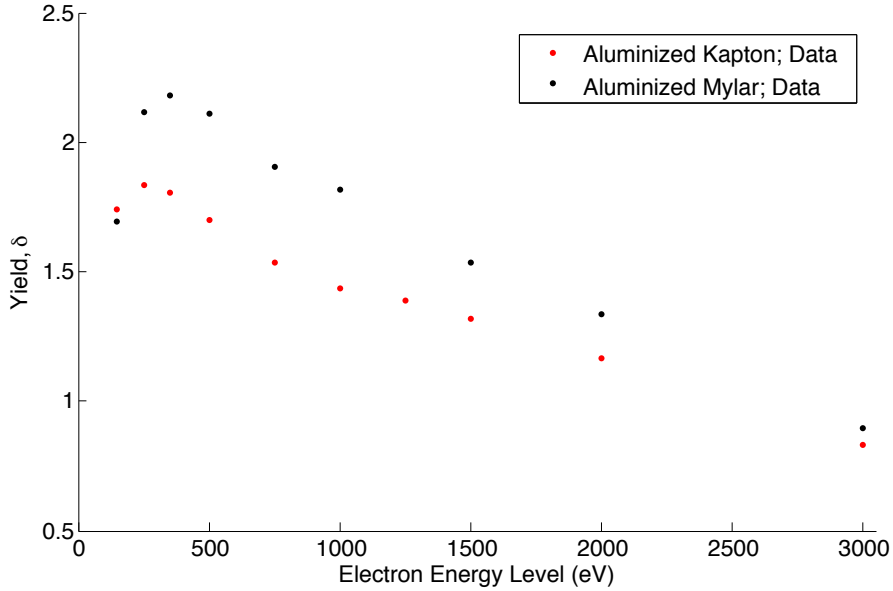

Figure 13: Comparison between experimental data for Aluminized Kapton and Aluminized Mylar

until energies are near 3000 eV. This shows that secondary electron emission is be a large factor in remote charging unless high beam energies are employed.

V. Application to EIMS

The results from this experiment yield important information about using the method of remote charging to raise the potential of a membrane structure for electrostatic inflation. Based on the secondary electron yield of a material, the achievable potential levels can vary by many kiloVolts. Thus, the difference between being able to obtain the desired potential level or not may be in the choice of materials. For example, in Figure 4 for the given GEO remote charging scenario, the aluminum object charged to an equilibrium potential of -8.8 kV while the Kapton material charged to -4.0 kV. Here, it may be more desirable to have a conducting material with a lower secondary electron emission. For

a membrane material, this could mean a thicker deposition layer of the aluminum onto the Kapton or Mylar, as a pure aluminum foil at membrane thicknesses does not have sufficient strength. Considering other charging methods, such as charge emission from the spacecraft, other materials may be more efficient for charging to desired high potentials. In the scenario of electron emission to charge positively, the higher the secondary electron emission (from plasma electrons), the easier it would be to charge positively. Even with remote charging using an electron beam, it could be possible to charge to positive potentials. Here, the beam energy would be chosen near the maximum of the yield curve in order to eject as many electrons with each incoming electron. The potential on the craft, however, would then be limited by the low energy of the electron beam.

VI. Conclusion

The focus of this paper is a study of the remote charging behavior of an electrostatically inflated membrane structure (EIMS). Specifically, the secondary electron emission is investigated though an experimental setup. The aim of the research is to better understand which materials would be more advantageous to reach the desired potential levels required for electrostatic inflation of a membrane space structure. An experimental setup to measure the secondary electron yield for a material is described and current results are presented. Presently, a discrepancy between the theoretical prediction for secondary emission of Nickel (with the Sternglass yield model) and the experimental data is being investigated. Preliminary yield curves for membrane materials are also presented. Yield curves for Aluminized Mylar and Aluminized Kapton show similar trends and magnitudes, both following the approximate trend of a Sternglass curve. Current results suggest that remote charging is feasible for membrane materials when beam energies are high. The next step in this research is to finalize secondary electron yield curves and better understand charging mechanics for EIMS applicable membrane materials.